ACS OMEGA

Open Access

http://pubs.acs.org/journal/acsodf

Article

Coactivation of Hydrogen Peroxide Using Pyrogenic Carbon and Magnetite for Sustainable Oxidation of Organic Pollutants

Yao Gui, Sen Guo, Ying Lv, Huiming Li, Junhuan Zhang, and Jianfa Li*

Cite This: *ACS Omega* 2024, 9, 6595−6605

Read Online

ACCESS | Metrics & More | Article Recommendations | Supporting Information

ABSTRACT: Pyrogenic carbon and magnetite (Fe_3O_4) were mixed together for the activation of hydrogen peroxide (H_2O_2), aiming to enhance the oxidation of refractory pollutants in a sustainable way. The experimental results indicated that the straw-derived carbon obtained by pyrolysis at 500−800 °C was efficient on coactivation of H_2O_2, and the most efficient one was that prepared at 700 °C (C700) featured with abundant defects. Specifically, the reaction rate constant (k_{obs}) for removal of an antibiotic ciprofloxacin in the coactivation system (C700/Fe_3O_4/H_2O_2) is 12.5 times that in the magnetite-catalyzed system (Fe_3O_4/H_2O_2). The faster pollutant oxidation is attributed to the sustainable production of $^{\bullet}OH$ in the coactivation process, in which the carbon facilitated decomposition of H_2O_2 and regeneration of Fe(II). Besides the enhanced H_2O_2 utilization in the coactivation process, the leaching of iron was controlled within the concentration limit in drinking water (0.3 mg·L^{-1}) set by the World Health Organization.

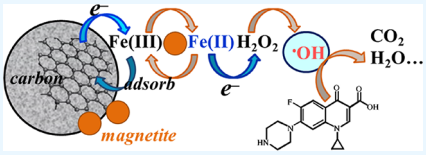

1. INTRODUCTION

Advanced oxidation processes (AOPs) using hydroxyl radical ($^{\bullet}OH$) as the major reactive oxygen species (ROS) are among the most powerful technologies for removal of refractory organic pollutants from water, because of the strong oxidation potential of $^{\bullet}OH$ ($E^{\theta}(^{\bullet}OH/H_2O)$ = 2.73 V) produced from activation of hydrogen peroxide (H_2O_2).[1,2] Iron sources, including both aqueous iron and solid iron minerals, are frequently used for triggering the Fenton reaction with H_2O_2 (eq 1).[3,4] Such Fenton/Fenton-like processes have advantages of easy availability of reactants, mild reaction conditions, simple operation, etc. Specifically, heterogeneous processes using iron minerals (e.g., magnetite, goethite, and hematite) can minimize the undesirable production of iron sludge waste that is a challenge for homogeneous Fenton processes.[5,6] Moreover, magnetite (Fe_3O_4) has been reported to be more reactive in mediating Fenton reaction than many other iron minerals.[7] However, the efficiency of such heterogeneous Fenton processes in oxidation of organic pollutants is bottlenecked by the unsustainable production of $^{\bullet}OH$ due to slow redox cycling of Fe(III)/Fe(II) (eq 2).[8,9] Thus, seeking for a simple solution to this problem is a topic of significance and many efforts have been made to accelerate the regeneration of Fe(II) using electron-rich materials.[10−12] For example, carbon materials such as graphene oxide[13] and carbon nanotubes[14,15] have been chosen for this purpose due to their good stability and electron transfer capability.

$$Fe(II) + H_2O_2 \rightarrow Fe(III) + {}^{\bullet}OH + OH^{-}(k_1 = 40 - 80 M^{-1}s^{-1}) \quad (1)$$

$$Fe(III) + H_2O_2 \rightarrow Fe(II) + HO_2^{\bullet} + H^{+}(k_2 = 0.0027 s^{-1}) \quad (2)$$

Pyrogenic carbon (e.g., biochar) is obtained naturally or artificially by pyrolysis of renewable biomass feedstock. It is cheaper and more easily available than the aforementioned carbonaceous materials. In addition to being a capable adsorbent of pollutant,[16,17] pyrogenic carbon can mediate electron transfer in redox reactions.[18−22] For example, biochar alone can activate H_2O_2[23,24] and persulfates[25,26] to produce ROS for oxidation of pollutants. However, the yield of $^{\bullet}OH$ from H_2O_2 decomposition in the biochar-activated system was less than 10% while H_2O and O_2 are the dominant products.[27,28] Thus, pyrogenic carbon was more often used as the supporting material of other active ingredients (e.g., iron nanoparticles) to enhance the performance of AOPs.[29−31] The supporting effect of carbon, such as dispersion of magnetic nanoparticles and/or enriching pollutants to the interfacial reaction sites, has been focused in the previous studies.[32,33] Co-activation of H_2O_2 using pyrogenic carbon and iron sources together provides a novel solution for the sustainable oxidation of organic pollutants, because pyrogenic carbon can mediate microbial reduction of Fe(III)[34−36] and may facilitate the regeneration of Fe(II) in Fenton reaction (eq 1). Thus, the enhanced oxidation efficiency of pollutants by coactivation of H_2O_2 using biochar and aqueous iron (Fe(III) or Fe(II)) has

Received: September 28, 2023
Revised: January 25, 2024
Accepted: January 26, 2024
Published: February 1, 2024

Table 1. Elemental Compositions and Specific Surface Areas of Carbon Samples

sample	N (%)	C (%)	H (%)	O (%)	H/C[a]	O/C[a]	ash (%)	SA ($m^2 \cdot g^{-1}$)
C300	1.22	54.5	5.48	10.2	1.21	0.140	19.6	5.37
C400	1.14	54.9	4.43	6.13	0.968	0.0837	24.2	13.9
C500	1.15	57.0	3.17	3.65	0.667	0.0480	27.4	57.5
C600	0.999	60.2	1.99	2.48	0.397	0.0309	29.5	117
C700	0.735	58.0	1.43	2.37	0.296	0.0306	30.8	193
C800	0.658	56.7	1.04	2.57	0.220	0.0340	33.2	275

[a]Molar ratios of the two elements.

been observed in our previous studies.[27,28] However, little is known about the performance of pyrogenic carbon on coactivation of H_2O_2 with magnetite, although magnetite has been reported to be a reactive iron mineral to catalyze Fenton reaction.

In this work, the pyrogenic carbon obtained by pyrolysis of rice straw at different temperatures (300−800 °C) was used for testing its performance in coactivation of H_2O_2 with magnetite and for exploring the relationship between the performance and the functional moieties of carbon. Herein, the pyrogenic carbon was mixed simply with magnetite so as to highlight the coactivation effect rather than the supporting effect of carbon. The target pollutants for evaluating this coactivation process are two common antibiotics (ciprofloxacin and sulfamethazine) that are frequently found in contaminated water and refractory to biodegradation. The objectives of this work are (1) to testify the coactivation effect between pyrogenic carbon and magnetite on oxidation of pollutants by H_2O_2, (2) to identify the functional moieties of pyrogenic carbon that made major contribution to the coactivation effect, and (3) to investigate the interactions between pyrogenic carbon and magnetite on coactivation of H_2O_2.

2. MATERIALS AND METHODS

2.1. Pyrogenic Carbon and Materials. The straw-derived carbon samples were prepared by slow pyrolysis of rice straw waste collected locally, following a procedure reported previously.[27] The carbon products were labeled as C300−C800, respectively, with the number suffix referring to the pyrolysis temperature (°C) for each sample. The elemental analysis (C, H, O, and N) of carbon was performed by using an elemental analyzer (EuroVector EA3000, Italy), and the oxygen content was measured with the oxygen analysis model in the same analyzer. The specific surface area (SA) was calculated using the Brunauer−Emmett−Teller (BET) method, based on the N_2 adsorption/desorption data obtained at 77K in a TriStar II3020 SA and porosity analyzer (Micromeritics, USA). The ash content was determined by heating the samples at 800 °C for 4 h. Fourier transform infrared spectra (FTIR) were recorded in the 4000−400 cm^{-1} region on a Nexus FTIR spectrophotometer (Nicolet, USA) using a KBr pellet. An Empyrean X-ray diffractometer (XRD) (Panalytical, Netherlands) was used to characterize the crystalline structure of samples. Electron paramagnetic resonance (EPR) measurement was performed on a Bruker A300 spectrometer (Germany), and the Raman spectra were recorded on a Renishaw inVia Raman spectrometer (UK). The cyclic voltammograms were measured using an electrochemical workstation (CHI660E, China).

The iron minerals (magnetite (Fe_3O_4) (99% purity), hematite (Fe_2O_3) (99% purity), and goethite (FeOOH) (99% purity)) are commercially available products purchased from Aladdin Agents Co., Ltd., China, and used in the following experiments without purification. Their specific SAs were measured to be 33.9, 2.78, and 25.6 $m^2 \cdot g^{-1}$ for magnetite, hematite, and goethite, respectively. Their surface morphology was observed with a JSM-6360LV scanning electron microscope (SEM) (JEOL, Japan) and included in Figure S1 of the online Supporting Information. Ciprofloxacin (98% purity), sulfamethazine (99%purity), and benzoic acid (BA) of analytical grade were purchased from Aladdin Agents Co. Ltd., China. Ferrous sulfate heptahydrate ($FeSO_4 \cdot 7H_2O$) of analytical grade used for preparing aqueous Fe(II) solution and H_2O_2 solution (30%, w/w) of analytical grade were purchased from the Sinopharm Chemical Reagent Co., Ltd., China. The 18.2 MΩ·cm (Milli-Q Gradient, Millipore, USA) pure water was used for preparing solutions.

2.2. Oxidation Experiments. The oxidation experiments were conducted in a conical flask in the dark in a thermostatic oscillator (KS4000i, IKA, Germany) running at a speed of 200 $r \cdot min^{-1}$ and a temperature of 25 ± 0.2 °C. Carbon was mixed with iron mineral by grinding in a porcelain mortar before use in the reaction system containing 100 mL of solution of pollutants (C_0 = 20 $mg \cdot L^{-1}$). The typical initial pH (pH_0) was adjusted to 3.0 ± 0.1 by using dilute H_2SO_4, and the oxidation reaction was initiated by the quick addition of H_2O_2. The typical dosages of H_2O_2, iron mineral, and carbon sample were 3.0 mM, 1.5 $g \cdot L^{-1}$, and 1.0 $g \cdot L^{-1}$, respectively, unless otherwise specified. At the predetermined reaction time (t, min), 0.7 mL of reaction solution was sampled and mixed into methanol of the same volume to quench the reaction. Then, the solution was filtered by a 0.22 μm membrane for subsequent analysis. All the experiments were conducted in triplicates. To test the reusability of the catalyst, the solid catalyst was separated by filtration out from the system after reaction and vacuum-dried before use in the next run. In one comparison study, the river water was used instead of pure water to prepare the ciprofloxacin solution used for oxidation experiments, so as to evaluate the applicability of catalyst in real water.[37] In another comparison study, an aqueous Fe(II) ($FeSO_4$) solution was used instead of iron mineral in oxidation experiments, so as to validate the contribution of dissolved iron to pollutant removal.

2.3. Analytical Methods. The residual concentrations of pollutants (C, $mg \cdot L^{-1}$) in solution samples were analyzed by using a high-performance liquid chromatography (HPLC) system (Shimadzu LC-20A, Japan) equipped with an ultraviolet detector at 275 nm. The separation was performed on an ODS-3 column (5 μm, 250 × 4.6 mm) with a flow rate of 1.0 $mL \cdot min^{-1}$ at 25 °C. The mobile phase was a mixture of acetonitrile and 0.025 mM H_3PO_4 (V/V = 17/83) for ciprofloxacin and a mixture of acetonitrile and 0.1% acetic acid (V/V = 40/60) for sulfamethazine, respectively. The $^{\bullet}OH$

https://doi.org/10.1021/acsomega.3c07525
ACS Omega 2024, 9, 6595−6605

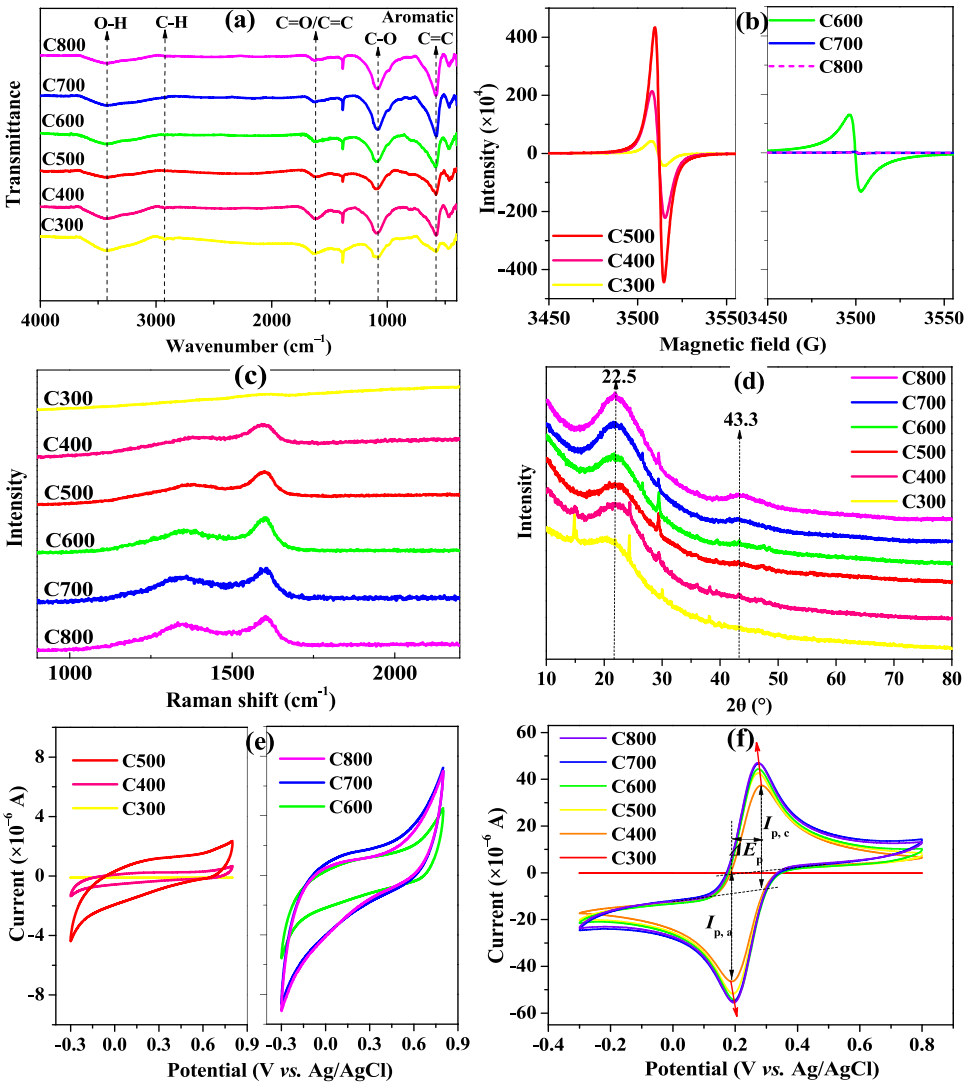

Figure 1. Characterizations of the carbon samples: (a) FTIR spectra, (b) EPR spectra, (c) Raman spectra, (d) XRD patterns, (e) cyclic voltammograms without probe, and (f) cyclic voltammograms using $K_3[Fe(CN)_6]$ as a probe.

production was detected on an EPR spectrometer (Bruker A300, Germany) using 5,5-dimethyl-1-pyrroline-*N*-oxide (DMPO) as the radical spin-trapping reagent. The accumulative production of $^{\bullet}OH$ in reaction systems was quantitatively measured using BA as a chemical probe.[38,39] The methods for measuring the residual H_2O_2 concentration, total organic carbon (TOC), total dissolved iron, and Fe(II) concentrations in solution samples can be found in our previous study.[27] The X-ray photoelectron spectra (XPS) were obtained using a Thermo Scientific K-Alpha XPS system (USA) with a monochromatic Al Kα source ($h\nu$ = 1486.6 eV), and the binding energies of photoelectrons were corrected by the C 1s peak at 284.8 eV.

3. RESULTS AND DISCUSSION

3.1. Functional Moieties and Electrochemical Properties of Carbon Samples. The elemental compositions and specific SAs of carbon samples are listed in Table 1. The carbon content in the samples was in the range of 54.5 to 60.2%, which is lower than the wood-derived carbon due to the high ash content derived from straw feedstock. The larger specific SA was observed on the carbon sample obtained at a higher pyrolysis temperature, which is consistent with that commonly observed in preparation of biomass-derived carbon products.

The activity of pyrogenic carbon in redox reactions, such as activation of H_2O_2 and persulfates, has been reported to depend on its functional moieties including oxygen-containing functional groups (OFGs), persistent free radicals (PFRs), and defects.[18,23,40,41] The OFGs (C═O, C−O, and −OH) along with aromatic C═C groups were observed by FTIR (Figure1a), indicating the quinonic/phenolic moieties in these carbon samples. The stronger aromatic C═C band and weaker −OH band observed in the samples prepared at higher temperatures (e.g., C700) reveal their higher aromaticity and fewer phenolic groups, which is consistent with the H/C and O/C ratios obtained by elemental analysis (Table 1). The intensity of the characteristic peaks in EPR spectra increased and then decreased with pyrolysis temperature, and the highest intensity was observed on the carbon prepared at 500 °C (C500), indicating that there are richest PFRs in this carbon. In contrast, there are hardly any PFRs detected in C700 and C800. Such change is in consistency with many previous studies about the influence of pyrolysis

https://doi.org/10.1021/acsomega.3c07525
ACS Omega 2024, 9, 6595−6605

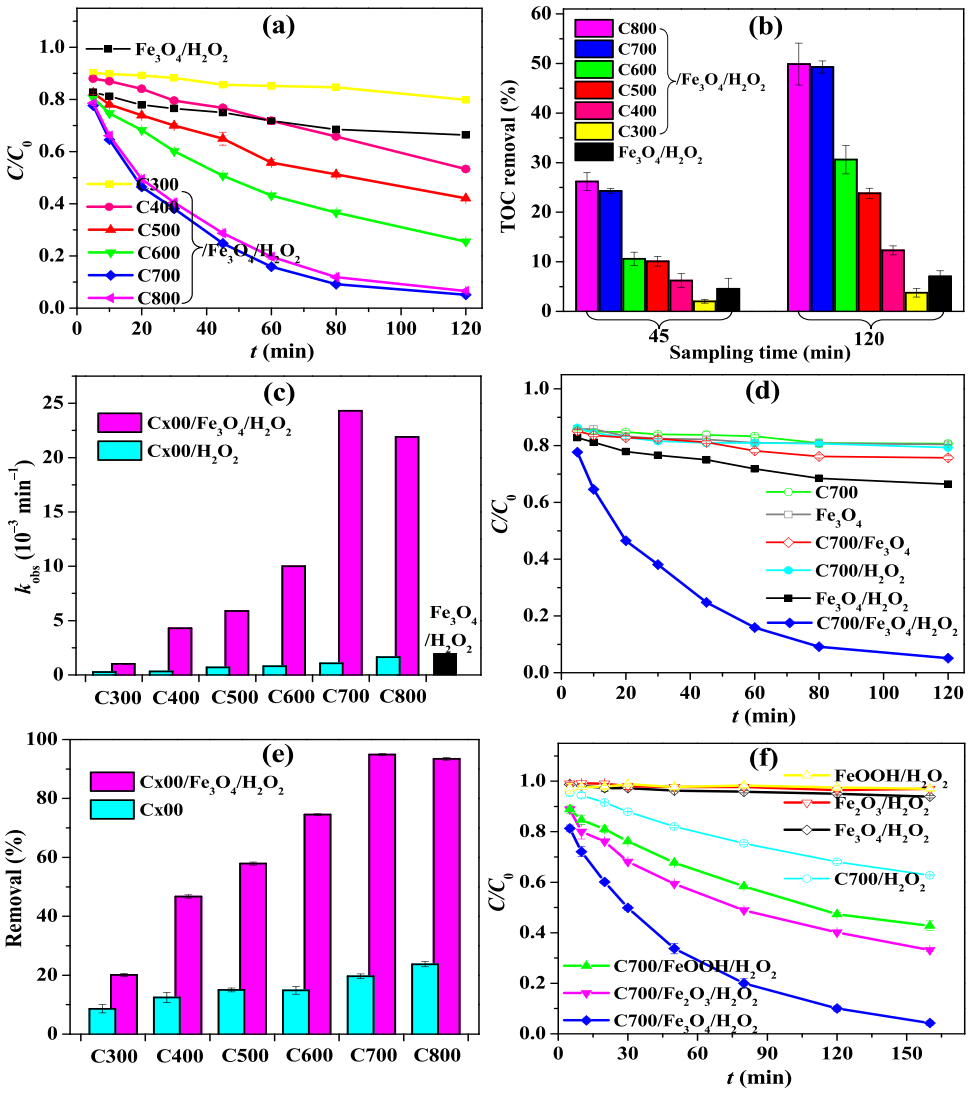

Figure 2. (a) Ciprofloxacin removal and (b) TOC removal in the coactivation systems using different carbons. (c) k_{obs} values for ciprofloxacin removal in coactivation systems vs carbon-activated systems. (d) Ciprofloxacin removal by various combinations of C700 with Fe_3O_4 and/or H_2O_2. (e) Ciprofloxacin removal after 120 min in coactivation systems vs adsorption by carbon alone. (f) Sulfamethazine removal by the coactivation systems using C700 and various iron minerals. Reaction conditions: [carbon] = 1.0 g·L^{-1}, [iron mineral: hematite (Fe_2O_3), magnetite (Fe_3O_4), and goethite (FeOOH)] = 1.5 g·L^{-1}, [H_2O_2] = 3.0 mM, and pH_0 = 3.0.

temperature on the richness of PFRs in carbon (biochar),[42,43] and the richest PFRs in C500 should be resulted from the stabilization of carbon-centered PFRs by adjacent oxygen atoms that acted as electron donors.[44] The *g*-factor was 2.0042 (>2.0040) for C300, indicating oxygen-centered radicals. The *g*-factors were 2.0040 for C400, 2.0038 for C500, and 2.0034 for C600. The values in the range of 2.0030−2.0040 indicate carbon-centered radicals with an adjacent oxygen atom. The *g*-factors were 2.0029 for C700 and 2.0028 for C800, indicating carbon-centered radicals (*g* value <2.0030).[23,44] The graphitization of and defects in carbon were evaluated by using Raman spectra (Figure 1c) and XRD analysis (Figure1d). The stronger D-band (~1350 cm^{-1}) was observed on the sample prepared at higher pyrolysis temperature, and the intensity ratios of D-band to G-band (~1600 cm^{-1}) (I_D/I_G) increased from 0.333 of C300, to 0.561 of C400, 0.609 of C500, 0.631 of C600, 0.785 of C700, and 0.825 of C800. The results indicate the higher graphitization degree and more abundant defects in the carbons prepared at higher pyrolysis temperatures.[41,45] The emerging band at 2θ = 43.3° and more salient band at 2θ = 22.5° in the XRD patterns (Figure 1d) of C700 and C800 further prove a more graphite-like structure in these pyrogenic carbons.[36,46]

The electrochemical properties related to the redox activity of carbon materials were accessed with cyclic voltammetry.[47] The much larger peak currents were observed on C700 and C800 (Figure 1e), implying their relatively stronger electron transfer capacity. In these two carbons, the higher peak currents ($I_{P,c}$ and $I_{P,a}$) and smaller difference between reduction and oxidation potentials (ΔE_P) were measured by using $K_3[Fe(CN)_6]$ as a probe (Figure 1f). For example, the ΔE_P of C800 is 0.078 V, which is apparently smaller than that of C400 (0.095 V). The higher peak currents and smaller ΔE_P indicate the relatively stronger electrical conductivity of pyrogenic carbon. Therefore, the carbons prepared at higher temperatures (C700 and C800) should have higher activity in redox reactions because of their high aromaticity, abundant defects, and graphite-like structure.

https://doi.org/10.1021/acsomega.3c07525
ACS Omega 2024, 9, 6595−6605

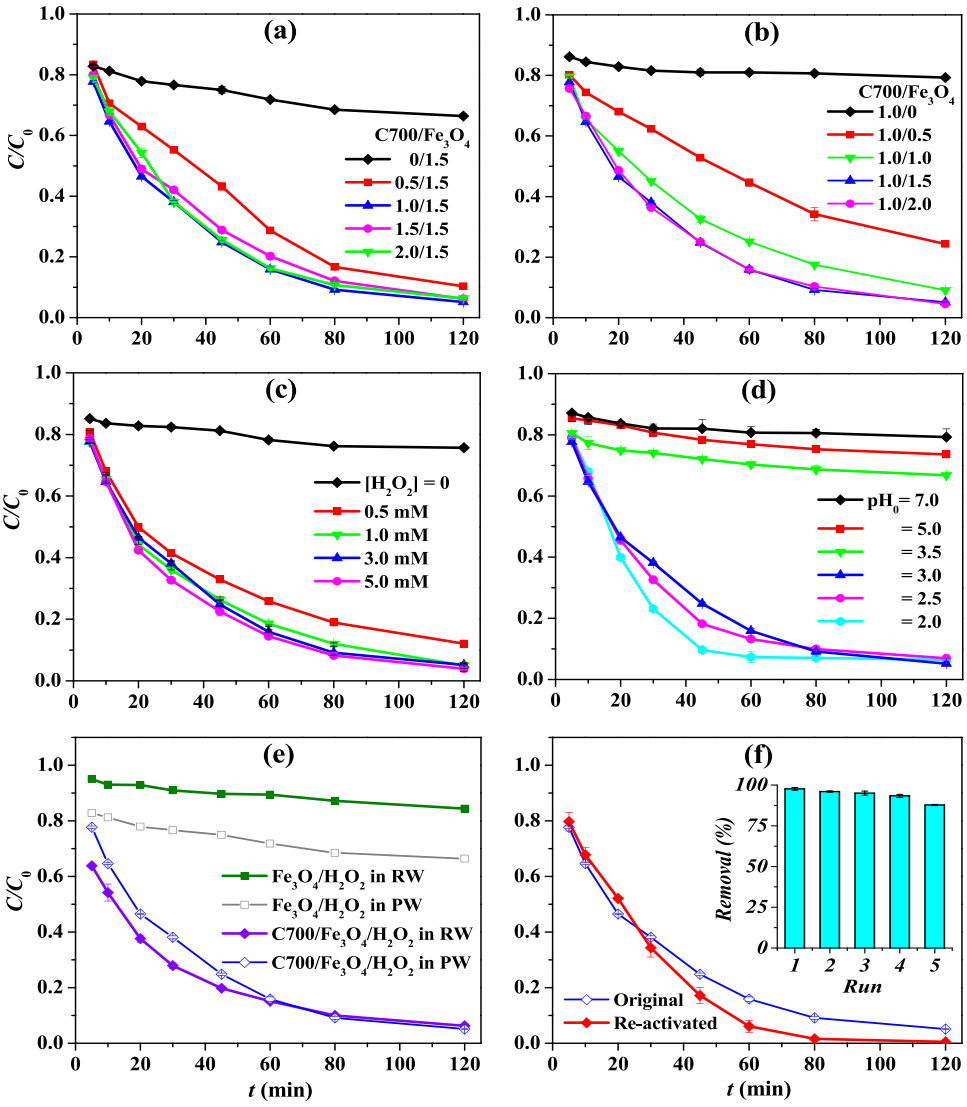

Figure 3. Ciprofloxacin removal by C700/Fe_3O_4/H_2O_2 at (a) different carbon dosages, (b) different magnetite dosages, (c) different H_2O_2 dosages, and (d) different pH_0. (e) Ciprofloxacin removal by C700/Fe_3O_4/H_2O_2 in river water (RW) and in pure water (PW). (f) Ciprofloxacin removal in repetitive experiments (inlet) and using reactivated cocatalysts by pyrolysis at 700 °C. Typical reaction conditions (except the variable): [C700] = 1.0 g·L^{-1}, [Fe_3O_4] = 1.5 g·L^{-1}, [H_2O_2] = 3.0 mM, and pH_0 = 3.0.

3.2. Coactivation Effect on Pollutant Removal. First, ciprofloxacin was used as the model pollutant to evaluate the performance of the coactivation systems using carbon samples obtained at different pyrolysis temperatures (C300−C800/Fe_3O_4/H_2O_2). Figure 2a shows the enhanced ciprofloxacin removal in all the coactivation systems except those using C300 and C400, in comparison with that in the heterogeneous Fenton system (Fe_3O_4/H_2O_2). The underperformance of C300 and C400 should be related to their weaker redox activity (Figure 1e,f). Among the other coactivation systems (C500−C800/Fe_3O_4/H_2O_2), the higher enhancement on ciprofloxacin removal was achieved using the carbon prepared at higher pyrolysis temperature, and the most dramatic enhancement was attained in those using C700 and C800 that have superior redox activity. The TOC removal in cocatalytic systems using various carbons (Figure2b) follows the same trend as that observed in ciprofloxacin removal; namely, more complete TOC removal was found in the system in which ciprofloxacin was degraded faster. Furthermore, in the elution diagrams of HPLC for analysis of pollutant concentration, the gradual disappearance of ciprofloxacin was accompanied by the appearance of degradation intermediates (Figures S2 and S3). Therefore, the ciprofloxacin removal is attributed dominantly to oxidation and mineralization that occurred in the coactivation process.

Second, the degradation rate of ciprofloxacin in the coactivation systems was calculated with the *pseudo*-first-order reaction rate model ($\ln(C/C_0) = -k_{obs}t$) and compared with that in the systems activated by carbon alone (C300−C800/H_2O_2) or by magnetite alone (Fe_3O_4/H_2O_2), so as to quantitatively evaluate the coactivation effect (Figure 2c). The much higher reaction rate constants (k_{obs}) were obtained in the coactivation systems using C700 (24.3×10^{-3} min^{-1} (R^2 = 0.995)) and C800 (21.9×10^{-3} min^{-1} (R^2 = 0.993)), which are 12.5 and 11.2 times those in the Fenton process (Fe_3O_4/H_2O_2), respectively. The k_{obs} values in the coactivation process using the carbons prepared at relatively high temperatures (C500−C800/Fe_3O_4/H_2O_2) were 8.35−22.7 times those in the corresponding carbon-activated system (C500−C800/H_2O_2). Apparently, the rapid degradation of pollutant in the

https://doi.org/10.1021/acsomega.3c07525
ACS Omega 2024, 9, 6595−6605

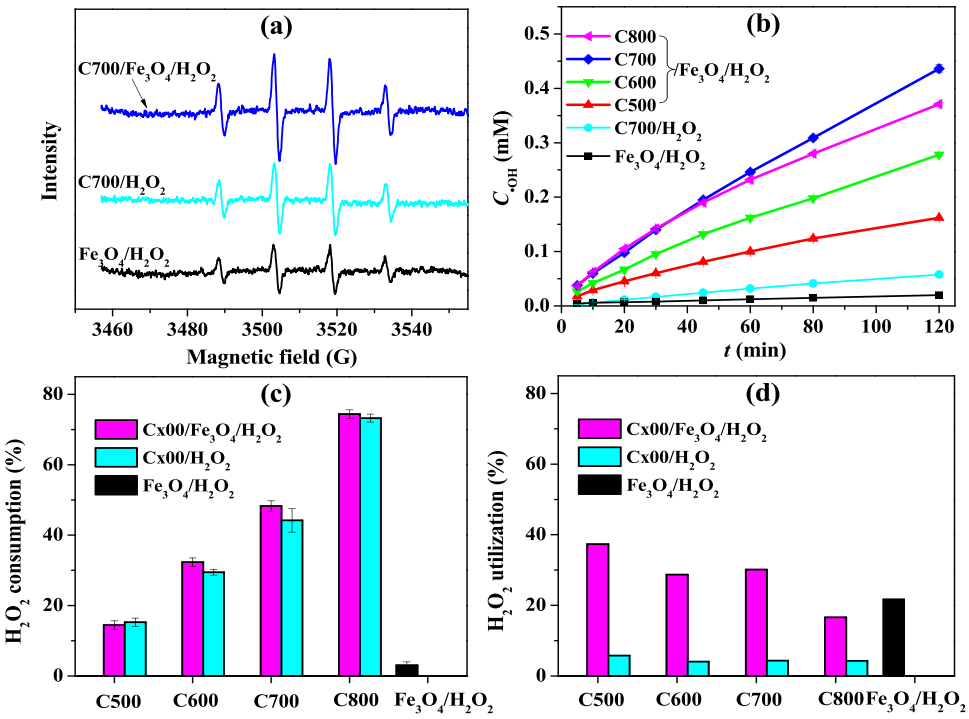

Figure 4. ROS in the cocatalytic systems: (a) EPR spectra of •OH trapped by DMPO, (b) accumulative •OH production, (c) consumption of H_2O_2 after 120 min of reaction, and (d) utilization efficiency of H_2O_2 calculated by molar •OH production per mole of consumed H_2O_2. Reaction conditions: [carbon] = 1.0 g·L^{-1}, [Fe_3O_4] = 1.5 g·L^{-1}, [H_2O_2] = 3.0 mM, and pH_0 = 3.0.

coactivation process is not just an additive result of the Fenton process and the carbon-activated process, proving the coactivation effect between pyrogenic carbon and magnetite.

Third, a comparison study using various combinations of C700 with Fe_3O_4 and/or H_2O_2 was performed with the results shown in Figure 2d. As expected, the fastest ciprofloxacin removal was observed in C700/Fe_3O_4/H_2O_2. The k_{obs} values in this coactivation system are 12.5 and 22.7 times those in Fe_3O_4/H_2O_2 and C700/H_2O_2, respectively, indicating a synergistic effect between carbon and magnetite on activation of H_2O_2. In addition, the results indicate a minor contribution from adsorption by C700 and/or magnetite to the total ciprofloxacin removal, despite the large SA of C700 (193 m^2·g^{-1}). Similarly, the adsorption by C800 having the largest SA (275 m^2·g^{-1}) did not make a major contribution to the overall ciprofloxacin removal in the coactivation system (Figure2e). The limited adsorption by C700 and C800 should be attributed first to the large molecular size of ciprofloxacin (13.5 × 3.0 × 7.4 Å). The N_2 adsorption isotherms of carbon samples (Figure S4) indicate their porosity dominated by micropores, which makes the internal surface difficult to be accessed by large-sized antibiotic molecules.[17,48] Second, the surfaces of C700 and C800 are positively charged at pH 3 according to their ζ potential values in suspension (+12.1 mV for C700 and +15.3 mV for C800, respectively), which is unfavorable for adsorption of protonated ciprofloxacin (pK_{a1} = 6.1) due to electrostatic repulsion. Furthermore, the XRD pattern of the C700 and magnetite mixture is the same as that of the pristine microsized magnetite (Figure S5), indicating that the mixing operation did not change the phase of magnetite. The particle size of magnetite after the mixing operation did not change either, according to the SEM observations (Figure S6). Therefore, the carbon's performance in enhancing oxidation of the pollutant in the coactivation process should not attribute mainly to the adsorption of pollutant or dispersion of magnetite.

Finally, two other iron minerals (hematite and goethite) were tested to prove the coactivation effect in removal of pollutants. The results in Figure 2f indicate that C700 is capable of accelerating the degradation of sulfamethazine in the Fenton process catalyzed by various iron minerals, although a different performance was observed for different iron minerals. The most complete sulfamethazine removal after a reaction of 160 min was observed in C700/Fe_3O_4/H_2O_2, confirming the relatively higher reactivity of magnetite than other iron minerals. The experimental results of removal of ciprofloxacin also indicate the much higher reactivity of magnetite than hematite and goethite on coactivation of H_2O_2 (Figure S7). The reason may be related to the inherent Fe(II) in magnetite that can readily initiate the Fenton reaction. Furthermore, the coactivation effect between carbon (C700) and magnetite was proved using other pollutants (an antibiotic sulfasalazine and a dye methyl orange) (Figure S8). In our previous study, a wood-derived biochar has been shown to be capable of accelerating the Fenton oxidation of a herbicide 2,4-D catalyzed by pyrite (an iron sulfide mineral).[39] Likewise, Liu et al.[49] reported that biochar accelerated the goethite-catalyzed Fenton-like oxidation of ofloxacin. Recently, the complementary effect on activation of H_2O_2 was observed between biochar and ferrihydrite (another iron mineral) for oxidation of sulfamethazine.[50] Therefore, the coactivation effect can be commonly found between pyrogenic carbon and various iron minerals and be applicable for oxidation of different organic pollutants.

3.3. Effect of Reaction Conditions and Reusability of Catalysts. The coactivation system using C700 (C700/Fe_3O_4/H_2O_2) was chosen for investigation on the effect of reaction conditions on pollutant removal. The results in Figure

https://doi.org/10.1021/acsomega.3c07525
ACS Omega 2024, 9, 6595−6605

3a,b indicate that the optimal dosages of C700 and magnetite were 1.0 and 1.5 g·L^{-1}, respectively, for the fast oxidation of ciprofloxacin. Fewer dosages of both carbon and magnetite resulted in slower oxidation of pollutant, while more carbon than 1.0 g·L^{-1} or more magnetite than 1.5 g·L^{-1} did not make the reaction much faster. At the optimal catalyst dosages, only 1.0 mM H_2O_2 was required for the efficient removal of 20 mg·L^{-1} of ciprofloxacin (Figure 3c). This H_2O_2 dosage is obviously lower than that used in ordinary Fenton processes (30−6000 mM)[51,52] and biochar-activated processes (10 mM)[53] and should be resulted from the high utilization of H_2O_2 in the coactivation process. Nevertheless, the efficiency of C700/Fe_3O_4/H_2O_2 on pollutant removal depends heavily on pH, just like that observed in the heterogeneous Fenton process.[54] The faster degradation of ciprofloxacin was observed at the lower pH (≤3.0), while the reaction became much slower at pH_0 >3.5 (Figure 3d). The results imply that the dissolved iron should play a crucial role in this process, as acidic pH is favorable for dissolution of iron from magnetite, which is discussed in Section 3.5. Except the significant influence of pH, the coactivation process showed to be adaptable to the change of solution chemistry, because the efficiency of C700/Fe_3O_4/H_2O_2 for ciprofloxacin removal did not change much when it was used in natural river water instead of pure water (Figure 3e). This outperformance should be related to the adsorption of cosolutes in real water by pyrogenic carbon.[26] Experiments using some typical coanions indicate that the removal of ciprofloxacin by C700/Fe_3O_4/H_2O_2 was not influenced by Cl^- but accelerated by NO_3^- and decelerated by HCO_3^- (Figure S9), because HCO_3^- is an interfering species of $^{\bullet}OH$.[55] Furthermore, the recycled catalyst mixture (C700/Fe_3O_4) showed good reusability in the repetitive experiments, although the efficiency of C700/Fe_3O_4/H_2O_2 on ciprofloxacin removal declined apparently in the fifth run (Figure 3f). However, after repyrolysis at 700 °C, the recycled catalyst mixture outperformed the original one on activation of H_2O_2 for oxidation of ciprofloxacin (Figure 3f). The reprolysis most likely reactivated the contaminated surface of carbon in the recycled catalyst mixture, because there was not apparent phase change of magnetite observed on both the recycled and the reactivated catalyst mixture (Figure S5). Therefore, the catalyst in this work can be simply prepared by mixing pyrogenic carbon and magnetite. The catalyst mixture was easily recycled after reaction and readily reactivated for repetitive use.

3.4. Sustainable Production of $^{\bullet}OH$ and Enhanced Utilization of H_2O_2. The low H_2O_2 dosage required in the coactivation system relies on the high yield of ROS from H_2O_2 decomposition. $^{\bullet}OH$ is the dominant ROS for degradation of pollutants in the coactivation system (C700/Fe_3O_4/H_2O_2), because addition of methanol as the $^{\bullet}OH$ scavenger almost ceased the reaction (Figure S10). EPR measurements further validated the dominant role of $^{\bullet}OH$, because the strong characteristic quartet (1:2:2:1) signals of $^{\bullet}OH$ were observed in the reaction systems (Figure 4a). The signals of carbon-centered radicals (e.g., hydroxymethyl radical ($^{\bullet}CH_2OH$)) rather than superoxide anion radicals ($O_2^{\bullet}$) were observed in the presence of methanol (Figure S11).[55] More importantly, the $^{\bullet}OH$ signals in C700/Fe_3O_4/H_2O_2 is stronger than that in C700/H_2O_2or Fe_3O_4/H_2O_2, implying more $^{\bullet}OH$ produced in the coactivation system. For proving this point, the accumulative $^{\bullet}OH$ production in various systems was quantified by using BA as a chemical probe. As expected, much more accumulative $^{\bullet}OH$ was measured in the coactivation systems using carbons produced at relatively high temperatures (C500−C800) than that in Fe_3O_4/H_2O_2 (Figure4b). Specifically, the accumulative $^{\bullet}OH$ produced in C700/Fe_3O_4/H_2O_2 after 120 min of reaction is 22.0 times that in Fe_3O_4/H_2O_2. When the extremely short life of $^{\bullet}OH$ (~10^{-6} s) is considered, its accumulation reflected by chemical probe should derive from the sustainable production by coactivation of H_2O_2. Furthermore, the accumulative $^{\bullet}OH$ produced in the coactivation systems using different carbons can be ranked in the order C800 ≈ C700 > C600 > C500, which is consistent with their efficiency on removal of pollutant (Figure 2). Moreover, only a few of the $^{\bullet}OH$ were produced in the systems using C300 and C400 (Figure S12), corresponding to their underperformance on ciprofloxacin removal.

The more $^{\bullet}OH$ produced in the coactivation system implies enhanced utilization of H_2O_2.[56] Figure 4c indicates that the H_2O_2 consumption in the coactivation system is comparable to the carbon-activated system using the same carbon. Thus, magnetite did not significantly influence the decomposed amount of H_2O_2, and pyrogenic carbon played a dominant role in inducing the decomposition of H_2O_2. However, the utilization efficiency of H_2O_2 in the carbon-activated system (without magnetite) is very low, although carbon has shown to be capable for activation of H_2O_2 in many previous studies.[23,24,53] The accumulative $^{\bullet}OH$ produced in the carbon-activated systems using various carbons (C500−C800/H_2O_2) is in the range of 0.0264−0.0942 mM after 120 min of reaction (Figure S13), which is far fewer than that in the corresponding coactivation systems (0.162−0.436 mM). When the utilization efficiency of H_2O_2 was calculated by the total $^{\bullet}OH$ production per molar consumption of H_2O_2, the high efficiency of 16.6−37.3% was obtained in the coactivation system (Figure 4d), which is 3.88−7.09 times that in the corresponding carbon-activated system. In addition, magnetite itself is not efficient in inducing the decomposition of H_2O_2 (Figure4c), as most of H_2O_2 remains unreacted in the magnetite-catalyzed Fenton process. These results thus demonstrate that the pyrogenic carbon (C500−C800) and magnetite are excellent partners for coactivation of H_2O_2, as carbons facilitated H_2O_2 decomposition while magnetite boosted $^{\bullet}OH$ production. Their cooperation kept the sustainable production of $^{\bullet}OH$ with a significantly enhanced utilization of H_2O_2. The similar boosted production of $^{\bullet}OH$ has been observed in the decomposition of H_2O_2 catalyzed by iron-rich biochar[57] and iron-impregnated biochar.[58] According to the characterizations of carbons (Figure 1), PFRs in C500 are dominant electron donors for production of $^{\bullet}OH$ from H_2O_2 decomposition[42] while the defects in C700 and C800 dominated the electron donation.[45] The higher capability of C700 and C800 on inducing H_2O_2 decomposition and consequent $^{\bullet}OH$ production in the coactivation system implies that defects in pyrogenic carbon are more powerful for boosting the efficiency of the magnetite-catalyzed Fenton process.

3.5. Interactions between Carbon and Magnetite. Heterogeneous Fenton reaction has been found to occur between H_2O_2 and iron species including both surface iron and dissolved iron.[59] Recently, Chen et al.[60] proposed that the oxidation of pollutants most likely occurred in the solid−liquid boundary layer, considering the extremely short life of $^{\bullet}OH$ and the mass transfer resistance from solution to surface. Wherever the reaction occurred, the pollutant removal by the

https://doi.org/10.1021/acsomega.3c07525
ACS Omega 2024, 9, 6595−6605

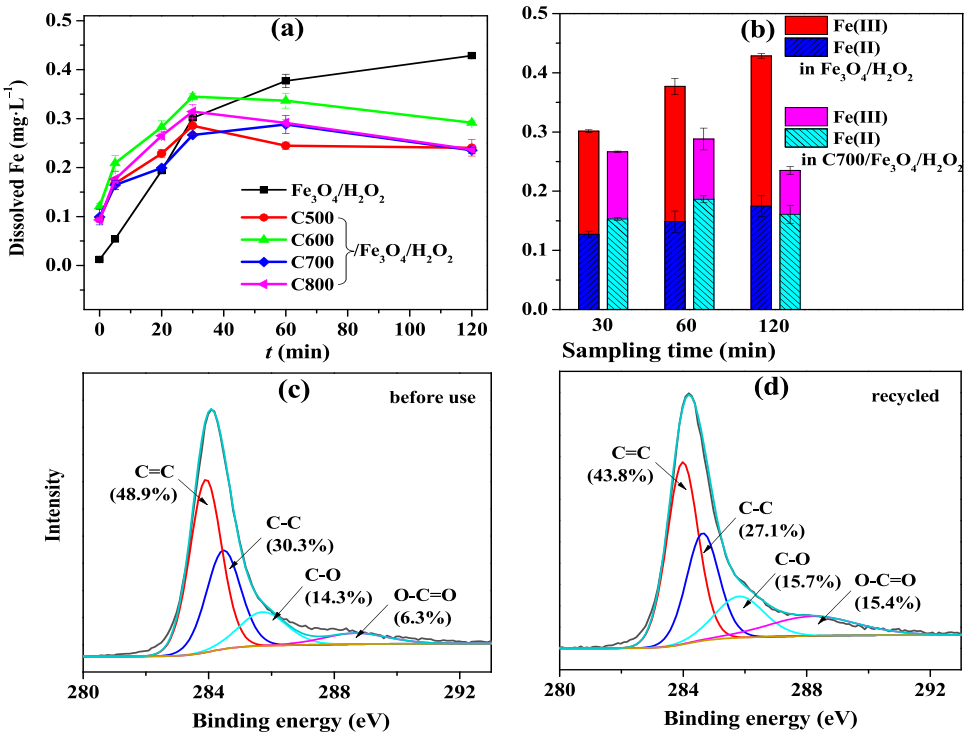

Figure 5. (a) Total dissolved iron in various reaction systems and (b) dissolved Fe(II) and Fe(III) species in Fe_3O_4/H_2O_2 and $C700/Fe_3O_4/H_2O_2$. C 1s XPS spectra of the $C700/Fe_3O_4$ catalyst: (c) before use and (d) recycled after reaction.

magnetite-catalyzed Fenton process was impeded by the sluggish production of $^{\bullet}OH$. The more sustainable $^{\bullet}OH$ production and faster oxidation of pollutant observed in the coactivation process should be attributed to the interactions between pyrogenic carbon and magnetite. First, the results in Figure 5a indicate that carbon induced the dissolution of iron from magnetite in the initial reaction stage. More dissolved iron was measured in the coactivation system than in the magnetite-catalyzed system before 20 min, and more dissolved iron was also observed in the suspensions of carbon and magnetite mixtures (without H_2O_2) than in magnetite suspension at pH_0 = 3.0 (Figure S14). The dissolved iron facilitated Fenton reaction in aqueous phase by reducing mass transfer resistance, so the faster oxidation of pollutant was observed at lower pH (Figure 3d) when more dissolved iron was measured in the coactivation process (Figure S15). Second, dissolved iron can be partially adsorbed by carbon. As can be seen in Figure 5a, the amount of dissolved iron in the coactivation systems remained at ~0.3 mg·L^{-1} after 30 min of reaction whereas more and continuously increasing dissolved iron was observed in Fe_3O_4/H_2O_2. Such a difference should result from the adsorption by carbon, which is proven by simply mixing carbon with a solution of ferric salt ($[Fe(III)]_0$ = 1.0 mg·L^{-1}). Only 0.83 mg·L^{-1} of aqueous iron was measured after addition of carbon (Figure S16), indicating that 17% of aqueous iron was adsorbed. Third, the pyrogenic carbon accelerated the regeneration of Fe(II). More aqueous Fe(II) was measured in $C700/Fe_3O_4/H_2O_2$ than that in Fe_3O_4/H_2O_2, despite the less amount of total dissolved iron (Fe(III)+Fe(II)) in the former system (Figure 5b). The reduction of Fe(III) by carbon has been reported previously in homogeneous Fenton-like systems[61,62] and was further proved by a significant amount of aqueous Fe(II) in the mixture of carbon and Fe(III) solution (Figure S16). The Fe(III)/Fe(II) cycle has also been reported to be accelerated by $O_2^{\bullet-}$.[63] However, in this study, the EPR signals of $O_2^{\bullet-}$ were not distinct enough to identify their contribution (Figure S11). Therefore, the pyrogenic carbon performed multiple functions in the coactivation process through interactions with magnetite. The fast release of iron from magnetite and then adsorption/desorption of aqueous iron by carbon bridged the electron donation/transfer from carbon, which accelerated the regeneration of Fe(II) and made Fenton reaction proceed sustainably. The defects and graphite-like structure in C700 and C800 are beneficial for electron donation/transfer, so more sustainable $^{\bullet}OH$ production and faster oxidation of pollutant were observed in the coactivation systems using these two carbons.

For further exploring the role of dissolved iron, C700 was mixed into the aqueous Fe(II) solution of a concentration (0.2 or 0.3 mg·L^{-1}) comparable to that measured in $C700/Fe_3O_4/H_2O_2$ and used for activation of H_2O_2 to degrade ciprofloxacin (Figure S17). As expected, the ciprofloxacin removal in $Fe(II)_{aq}/C700/H_2O_2$ is much faster than that in $C700/H_2O_2$, confirming the significant contribution from the dissolved iron to Fenton reaction. Nevertheless, the degradation of ciprofloxacin in $Fe(II)_{aq}/C700/H_2O_2$ is still slower than that in $C700/Fe_3O_4/H_2O_2$, indicating the potential occurrence of the Fenton reaction involving surface Fe(II). The interactions between carbon and magnetite were further proved by XPS analysis. The band belonging to O−C═O groups in the C 1s spectra became stronger for the recycled $C700/Fe_3O_4$ catalyst (Figure 5c,d), validating the oxidation of the carbon surface.[37]

What deserves emphasis is that the pyrogenic carbon can regulate the leaching of iron in the coactivation process by adsorption of aqueous iron and control its concentration within 0.3 mg·L^{-1} after reaction (Figure 5a). This concen-

https://doi.org/10.1021/acsomega.3c07525
ACS Omega 2024, 9, 6595−6605

tration is equal to the upper limit of dissolved iron in drinking water set by the World Health Organization (WHO) and is much lower than the leached iron from magnetite-catalyzed Fenton process reported previously.[64] In addition, the production of iron sludge in the Fenton process is negligible at such a low concentration of aqueous iron (0.3−1.0 mg·L^{-1}) according to our previous studies.[27,62] Thus, the sustainability of the oxidation process is enhanced in view of waste disposal as well.

4. CONCLUSIONS

The research demonstrated that the carbon produced by pyrolysis at temperature ranging from 500 to 800 °C was efficient for coactivation of H_2O_2 with magnetite, so as to keep the sustainable production of •OH and then promote the oxidation of organic pollutants. The performance of carbon samples in coactivation of H_2O_2 relies on their functional moieties. The pyrogenic carbon facilitated H_2O_2 decomposition and accelerated the regeneration of Fe(II) in the coactivation process. Its mixture with magnetite improved the utilization efficiency of H_2O_2, so that efficient oxidation of pollutants was achieved at a low H_2O_2 dosage (1.0 mM). Furthermore, the carbon controlled the leaching of iron from magnetite into the aqueous phase within the concentration limit in drinking water set by WHO, which makes this coactivation process more environmentally friendly than the ordinary Fenton process. Finally, these benefits of pyrogenic carbon can be achieved by simply mixing with commercially available iron minerals (e.g., magnetite), which makes it superior to those synthesized composite catalysts in view of cost and sustainability and provides a cheap and feasible method to improve the performance of AOPs.

■ ASSOCIATED CONTENT

Supporting Information

The Supporting Information is available free of charge at https://pubs.acs.org/doi/10.1021/acsomega.3c07525.

SEM images of iron minerals, identification of the degradation intermediates, N_2 adsorption/desorption isotherms of carbons, XRD patterns and SEM images of magnetite and its mixture with carbon, removal of different pollutants using various iron minerals, ciprofloxacin removal using methanol as •OH scavenger, EPR spectra of radicals trapped by DMPO and methanol, accumulative •OH production in the carbon-activated systems, dissolved iron species, and ciprofloxacin removal in $Fe(II)_{aq}$/C700/H_2O_2 (PDF)

■ AUTHOR INFORMATION

Corresponding Author

Jianfa Li − *College of Chemistry and Chemical Engineering, Shaoxing University, Shaoxing 312000 Zhejiang, China;* orcid.org/0000-0002-0876-4094; Email: ljf@usx.edu.cn

Authors

Yao Gui − *College of Chemistry and Chemical Engineering, Shaoxing University, Shaoxing 312000 Zhejiang, China*

Sen Guo − *College of Chemistry and Chemical Engineering, Shaoxing University, Shaoxing 312000 Zhejiang, China*

Ying Lv − *College of Chemistry and Chemical Engineering, Shaoxing University, Shaoxing 312000 Zhejiang, China*

Huiming Li − *College of Chemistry and Chemical Engineering, Shaoxing University, Shaoxing 312000 Zhejiang, China*

Junhuan Zhang − *College of Chemistry and Chemical Engineering, Shaoxing University, Shaoxing 312000 Zhejiang, China*

Complete contact information is available at: https://pubs.acs.org/10.1021/acsomega.3c07525

Notes

The authors declare no competing financial interest.

■ ACKNOWLEDGMENTS

This work was supported by the National Natural Science Foundation of China (No. 21777103).

■ REFERENCES

(1) Pignatello, J. J.; Oliveros, E.; Mackay, A. Advanced oxidation processes for organic contaminant destruction based on the Fenton reaction and related chemistry. *Crit. Rev. Env. Sci. Tec.* **2006**, *36*, 1−84.

(2) Diao, Z.-H.; Liu, J.-J.; Hu, Y.-X.; Kong, L.-J.; Jiang, D.; Xu, X.-R. Comparative study of Rhodamine B degradation by the systems pyrite/H_2O_2 and pyrite/persulfate: Reactivity, stability, products and mechanism. *Sep. Purif. Technol.* **2017**, *184*, 374−383.

(3) Zhu, Y.; Zhu, R.; Xi, Y.; Zhu, J.; Zhu, G.; He, H. Strategies for enhancing the heterogeneous Fenton catalytic reactivity: A review. *Appl. Catal. B: Environ.* **2019**, *255*, No. 117739.

(4) Zhu, Y.; Xie, Q.; Deng, F.; Ni, Z.-B.; Lin, Q.-Q.; Cheng, L.-L.; Chen, X.-J.; Qiu, R.-L.; Zhu, R.-L. The differences in heterogeneous Fenton catalytic performance and mechanism of various iron minerals and their influencing factors: A review. *Sep. Purif. Technol.* **2023**, *325*, No. 124702.

(5) Hussain, S.; Aneggi, E.; Maschio, S.; Contin, M.; Goi, D. Steel scale waste as a heterogeneous Fenton-like catalyst for the treatment of landfill leachate. *Ind. Eng. Chem. Res.* **2021**, *60*, 11715−11724.

(6) Chen, L.; Yang, Z.-C.; Qian, J.-S.; Pan, B.-C. Interaction between organic compounds and catalyst steers the oxidation pathway and mechanism in the iron oxide-based heterogeneous Fenton system. *Environ. Sci. Technol.* **2022**, *56*, 14059−14068.

(7) Munoz, M.; de Pedro, Z. M.; Casas, J. A.; Rodriguez, J. J. Preparation of magnetite-based catalysts and their application in heterogeneous Fenton oxidation − a review. *Appl. Catal. B: Environ.* **2015**, *176*, 249−265.

(8) Agu, U. A.; Mendieta, S. N.; Gerbaldo, M. V.; Crivello, M. E.; Casuscelli, S. G. Highly active heterogeneous Fenton-like system based on cobalt ferrite. *Ind. Eng. Chem. Res.* **2020**, *59*, 1702−1711.

(9) Xiao, J.; Lai, J.-H.; Li, R.-C.; Fang, X.; Zhang, D.-F.; Tsiakaras, P.; Wang, Y. Enhanced ultrasonic-assisted heterogeneous Fenton degradation of organic pollutants over a new copper magnetite (Cu-Fe_3O_4/Cu/C) nanohybrid catalyst. *Ind. Eng. Chem. Res.* **2020**, *59*, 12431−12440.

(10) Hou, X.-J.; Huang, X.-P.; Jia, F.-L.; Ai, Z.-H.; Zhao, J.-C.; Zhang, L.-Z. Hydroxylamine promoted goethite surface Fenton degradation of organic pollutants. *Environ. Sci. Technol.* **2017**, *51*, 5118−5126.

(11) Sun, H.-W.; Xie, G.-H.; He, D.; Zhang, L.-Z. Ascorbic acid promoted magnetite Fenton degradation of alachlor: Mechanistic insights and kinetic modeling. *Appl. Catal. B: Environ.* **2020**, *267*, No. 118383.

(12) Zhou, H.-Y; Zhang, H.; He, Y.-L.; Huang, B.-K.; Zhou, C.-Y.; Yao, G.; Lai, B. Critical review of reductant-enhanced peroxide activation processes: Trade-off between accelerated Fe^{3+}/Fe^{2+} cycle and quenching reactions. *Appl. Catal. B: Environ.* **2021**, *286*, No. 119900.

(13) Moztahida, M.; Nawaz, M.; Kim, J.; Shahzad, A.; Kim, S.; Jang, J.; Lee, D. S. Reduced graphene oxide-loaded-magnetite: A Fenton-like heterogeneous catalyst for photocatalytic degradation of 2-methylisoborneol. *Chem. Eng. J.* **2019**, *370*, 855−865.

(14) Zhu, R.-L.; Zhu, Y.-P.; Xian, H.-Y.; Yan, L.-X.; Fu, H.-Y.; Zhu, G.-Q.; Xi, Y.-F.; Zhu, J.-X.; He, H.-P. CNTs/ferrihydrite as a highly efficient heterogeneous Fenton catalyst for the degradation of bisphenol A: The important role of CNTs in accelerating Fe(III)/Fe(II) cycling. *Appl. Catal. B: Environ.* **2020**, *270*, No. 118891.
(15) Zhou, C.-Y.; Zhou, P.; Sun, M.-L.; Liu, Y.; Zhang, H.; Xiong, Z.-K.; Liang, J.; Duan, X.-G.; Lai, B. Nitrogen-doped carbon nanotubes enhanced Fenton chemistry: Role of near-free iron (III) for sustainable iron (III)/iron (II) cycles. *Water Res.* **2022**, *210*, No. 117984.
(16) Pignatello, J. J.; Mitch, W. A.; Xu, W.-Q. Activity and reactivity of Pyrogenic carbonaceous matter toward organic compounds. *Environ. Sci. Technol.* **2017**, *51*, 8893−8908.
(17) Zhu, X.-X.; Li, C.-Y.; Li, J.-F.; Xie, B.; Lü, J.-H.; Li, Y.-M. Thermal treatment of biochar in the air/nitrogen atmosphere for developed mesoporosity and enhanced adsorption to tetracycline. *Bioresour. Technol.* **2018**, *263*, 475−482.
(18) Sun, T.; Levin, B. D.; Schmidt, M. P.; Guzman, J. J.; Enders, A.; Martinez, C. E.; Muller, D. A.; Angenent, L. T.; Lehmann, J. Simultaneous quantification of electron transfer by carbon matrices and functional groups in Pyrogenic carbon. *Environ. Sci. Technol.* **2018**, *52*, 8538−8547.
(19) Wan, Z.-H.; Sun, Y.-Q.; Tsang, D. C.; Hou, D.-Y.; Cao, X.-D.; Zhang, S.-C.; Gao, B.; Ok, Y.-S. Sustainable remediation with an electroactive biochar system: mechanisms and perspectives. *Green Chem.* **2020**, *22*, 2688−2711.
(20) Nidheesh, P. V.; Gopinath, A.; Ranjith, N.; Praveen Akre, A.; Sreedharan, V.; Suresh Kumar, M. Potential role of biochar in advanced oxidation processes: A sustainable approach. *Chem. Eng. J.* **2021**, *405*, No. 126582.
(21) Wang, D.-X.; Huang, D.-Y.; Wu, S.; Fang, G.-D.; Zhu, F.-X.; Chen, N.; Liu, S.-C.; Zhu, C.-Y.; Zhou, D.-M. Pyrogenic carbon initiated the generation of hydroxyl radicals from the oxidation of sulfide. *Environ. Sci. Technol.* **2021**, *55*, 6001−6011.
(22) Xu, Z.-B.; Yu, Y.-L.; Xu, X.-Y.; Tsang, D. C. W.; Yao, C.-B.; Fan, J.; Zhao, L.; Qiu, H.; Cao, X.-D. Direct and indirect electron transfer routes of chromium(VI) reduction with different crystalline ferric oxyhydroxides in the presence of Pyrogenic carbon. *Environ. Sci. Technol.* **2022**, *56*, 1724−1735.
(23) Fang, G.-D.; Gao, J.; Liu, C.; Dionysiou, D. D.; Wang, Y.; Zhou, D.-M. Key role of persistent free radicals in hydrogen peroxide activation by biochar: Implications to organic contaminant degradation. *Environ. Sci. Technol.* **2014**, *48*, 1902−1910.
(24) Luo, K.; Yang, Q.; Pang, Y.; Wang, D.-B.; Li, X.; Lei, M.; Huang, Q. Unveiling the mechanism of biochar-activated hydrogen peroxide on the degradation of ciprofloxacin. *Chem. Eng. J.* **2019**, *374*, 520−530.
(25) Zhu, S.-S.; Huang, X.-C.; Ma, F.; Wang, L.; Duan, X.-G.; Wang, S.-B. Catalytic removal of aqueous contaminants on n-doped graphitic biochars: Inherent roles of adsorption and nonradical mechanisms. *Environ. Sci. Technol.* **2018**, *52*, 8649−8658.
(26) Hung, C.-M.; Chen, C.-W.; Huang, C.-P.; Dong, C.-D. N-doped metal-free biochar activation of peroxymonosulfate for enhancing the degradation of antibiotics sulfadiazine from aquaculture water and its associated bacterial community composition. *J. Environ. Chem. Eng.* **2022**, *10*, No. 107172.
(27) Feng, D.-Q.; Lü, J.-H.; Guo, S.; Li, J.-F. biochar enhanced the degradation of organic pollutants through a Fenton process using trace aqueous iron. *J. Environ. Chem. Eng.* **2021**, *9*, No. 104677.
(28) Lai, M.-N.; Li, J.-F.; Li, H.-M.; Gui, Y.; Lü, J.-H. Adsorption-reduction of Fe(III) by different biochars and their co-activation of H_2O_2 for oxidation of refractory pollutants. *Catal. Commun.* **2023**, *176*, No. 106626.
(29) Dong, C.-D.; Chen, C.-W.; Tsai, M.-L.; Chang, J.-H.; Lyu, S.-Y.; Hung, C.-M. Degradation of 4-nonylphenol in marine sediments by persulfate over magnetically modified biochars. *Bioresour. Technol.* **2019**, *281*, 143−148.
(30) Li, L.; Lai, C.; Huang, F.-L.; Cheng, M.; Zeng, G.-M.; Huang, D.-L.; Li, B.-S.; Liu, S.-Y.; Zhang, M.-M.; Qin, L.; Li, M.-F.; He, J.-F.; Zhang, Y.-J.; Chen, L. Degradation of naphthalene with magnetic bio-char activate hydrogen peroxide: synergism of bio-char and Fe-Mn binary oxides. *Water. Res.* **2019**, *160*, 238−248.
(31) Dong, F.-X.; Yan, L.; Huang, S.-T.; Liang, J.-Y.; Zhang, W.-X.; Yao, X.-W.; Chen, X.; Qian, W.; Guo, P.-R.; Kong, L.-J.; Chu, W.; Diao, Z.-H. Removal of antibiotics sulfadiazine by a biochar based material activated persulfate oxidation system: Performance, products and mechanism. *Process Saf. Environ. Protect.* **2022**, *157*, 411−419.
(32) Wang, C.-Q.; Sun, R.-R.; Huang, R. Highly dispersed iron-doped biochar derived from sawdust for Fenton-like degradation of toxic dyes. *J. Clean Prod.* **2021**, *297*, No. 126681.
(33) Liu, H.-R.; Liu, Y.-K.; Li, X.; Zheng, X.-Y.; Feng, X.-Y.; Yu, A.-C. Adsorption and Fenton-like degradation of ciprofloxacin using corncob biochar-based magnetic iron−copper bimetallic nanomaterial in aqueous solutions. *Nanomaterials* **2022**, *12*, 579.
(34) Klüpfel, L.; Keiluweit, M.; Kleber, M.; Sander, M. Redox properties of plant biomass-derived black carbon (biochar). *Environ. Sci. Technol.* **2014**, *48*, 5601−5611.
(35) Wu, S.; Wang, D.-J.; Liu, c.; Fang, G.-D.; Sun, T.-Y.; Cui, P.-X.; Yan, H.-J.; Wang, Y.-J.; Zhou, D.-M. Pyridinic- and pyrrolic nitrogen in Pyrogenic carbon improves electron shuttling during microbial Fe (III) reduction. *ACS Earth Space Chem.* **2021**, *5*, 900−909.
(36) Yu, W.-T.; Chu, C.-H.; Chen, B.-L. Enhanced microbial ferrihydrite reduction by Pyrogenic carbon: impact of graphitic structures. *Environ. Sci. Technol.* **2022**, *56*, 239−250.
(37) Lai, M.-N.; Li, J.-F.; Li, H.-M.; Gui, Y.; Lü, J.-H. N,S-codoped biochar outperformed N-doped biochar on co-activation of H_2O_2 with trace dissolved Fe(III) for enhanced oxidation of organic pollutants. *Environ. Pollut.* **2023**, *334*, No. 122208.
(38) Tong, M.; Yuan, S.-H.; Ma, S.-C.; Jin, M.-J.; Liu, D.; Cheng, D.; Liu, X.-X.; Gan, Y.-Q.; Wang, Y.-X. Production of abundant hydroxyl radicals from oxygenation of subsurface sediments. *Environ. Sci. Technol.* **2016**, *50*, 214−221.
(39) Zhu, X.-X.; Li, J.-F.; Xie, B.; Feng, D.-Q.; Li, Y.-M. Accelerating effects of biochar for pyrite-catalyzed Fenton-like oxidation of herbicide 2,4-D. *Chem. Eng. J.* **2020**, *391*, No. 123605.
(40) He, J.; Xiao, Y.; Tang, J.-C.; Chen, H.-K.; Sun, H.-W. Persulfate activation with sawdust biochar in aqueous solution by enhanced electron donor-transfer effect. *Sci. Total Environ.* **2019**, *690*, 768−777.
(41) Ouyang, D.; Chen, Y.; Yan, J.-C.; Qian, L.-B.; Han, L.; Chen, M.-F. Activation mechanism of peroxymonosulfate by biochar for catalytic degradation of 1,4-dioxane: Important role of biochar defect structures. *Chem. Eng. J.* **2019**, *370*, 614−624.
(42) Yang, J.; Pan, B.; Li, H.; Liao, S.-H.; Zhang, D.; Wu, M.; Xing, B.-H. Degradation of p-nitrophenol on biochars: Role of persistent free radicals. *Environ. Sci. Technol.* **2016**, *50*, 694−700.
(43) Luo, K.; Pang, Y.; Wang, D.-B.; Li, X.; Wang, L.-P.; Lei, M.; Huang, Q.; Yang, Q. A critical review on the application of biochar in environmental pollution remediation: Role of persistent free radicals (PFRs). *J. Environ. Sci.* **2021**, *108*, 201−216.
(44) Deng, R.; Luo, H.; Huang, D.; Zhang, C. biochar-mediated Fenton-like reaction for the degradation of sulfamethazine: Role of environmentally persistent free radicals. *Chemosphere* **2020**, *255*, No. 126975.
(45) Wang, T.; Xue, L.; Liu, Y.-H.; Fang, T.; Zhang, L.; Xing, B.-S. Insight into the significant contribution of intrinsic defects of carbon-based materials for the efficient removal of tetracycline antibiotics. *Chem. Eng. J.* **2022**, *435*, No. 134822.
(46) Xiao, X.; Chen, B.-L.; Chen, Z.-M.; Zhu, L.-Z.; Schnoor, J. L. Insight into multiple and multilevel structures of biochars and their potential environmental applications: A critical review. *Environ. Sci. Technol.* **2018**, *52*, 5027−5047.
(47) Sun, T.; Levin, B. D.; Guzman, J. J.; Enders, A.; Muller, D. A.; Angenent, L. T.; Lehmann, J. Rapid electron transfer by the carbon matrix in natural Pyrogenic carbon. *Nat. Commun.* **2017**, *8*, 14873.
(48) Li, C.-Y.; Zhu, X.-X.; He, H.-L.; Fang, Y. X.; Dong, H. P.; Lü, J.-H.; Li, J.-F.; Li, Y.-M. Adsorption of two antibiotics on biochar prepared in air-containing atmosphere: Influence of biochar porosity and molecular size of antibiotics. *J. Mol. Liq.* **2019**, *274*, 353−361.

https://doi.org/10.1021/acsomega.3c07525
ACS Omega 2024, 9, 6595−6605

(49) Liu, G.-F.; Zhang, Y.-Y.; Yu, H.-L.; Jin, R.-F.; Zhou, J.-T. Acceleration of goethite-catalyzed Fenton-like oxidation of ofloxacin by biochar. *J. Hazard. Mater.* **2020**, *397*, No. 122783.
(50) Guo, S.; Shen, C.; Gui, Y.; Li, H.-M.; Lü, J.-H.; Li, J.-F. The complementary effect between biochar and ferrihydrite in sustainable Fenton-like oxidation of pollutant. *J. Saudi Chem. Soc.* **2023**, *27*, No. 101684.
(51) Xing, M.-Y.; Xu, W.-J.; Dong, C.-C.; Bai, Y.-C.; Zeng, J.-B.; Zhou, Y.; Zhang, J.-L.; Yin, Y.-D. Metal sulfides as excellent co-catalysts for H_2O_2 decomposition in advanced oxidation processes. *Chem.* **2018**, *4*, 1359−1372.
(52) Wang, X.-P.; Liu, W.; Qin, J.-Y.; Lei, L.-C. Improvement of H_2O_2 utilization by the persistent heterogeneous Fenton reaction with the Fe_3O_4-zeolite-cyclodextrin composite. *Ind. Eng. Chem. Res.* **2020**, *59*, 2192−2202.
(53) Huang, D.-L.; Wang, Y.; Zhang, C.; Zeng, G. M.; Lai, C.; Wan, J.; Qin, L.; Zeng, Y.-L. Influence of morphological and chemical features of biochar on hydrogen peroxide activation: implications on sulfamethazine degradation. *RSC Adv.* **2016**, *6*, 73186−73196.
(54) Chen, Y.-F.; Miller, C. J.; Waite, T. D. pH dependence of hydroxyl radical, ferryl, and/or ferric peroxo species generation in the heterogeneous Fenton process. *Environ. Sci. Technol.* **2022**, *56*, 1278−1288.
(55) Schneider, J. T.; Firak, D. S.; Ribeiro, R. R.; Peralta-Zamora, P. Use of scavenger agents in heterogeneous photocatalysis: truths, half-truths, and misinterpretations. *Phys. Chem. Chem. Phys.* **2020**, *22*, 15723−15733.
(56) Zhang, T.; Wen, Y.; Pan, Z.; Kuwahara, Y.; Mori, K.; Yamashita, H.; Zhao, Y.; Qian, X. Overcoming acidic H_2O_2/Fe(II/III) redox-induced low H_2O_2 utilization efficiency by carbon quantum dots Fenton-like catalysis. *Environ. Sci. Technol.* **2022**, *56*, 2617−2625.
(57) Tao, S.-Y.; Liang, S.; Chen, Y.; Yu, W.-B.; Hou, H.-J.; Qiu, J.-J.; Zhu, Y.-W.; Xiao, K.-K.; Hu, J.-P.; Liu, B.-C.; Wang, Y.-F.; Yang, J.-K. Enhanced sludge dewaterability with sludge-derived biochar activating hydrogen peroxide: Synergism of Fe and Al elements in biochar. *Water Res.* **2020**, *182*, No. 115927.
(58) Zhang, X.; Sun, P.; Wei, K.; Huang, X.; Zhang, X. Enhanced H_2O_2 activation and sulfamethoxazole degradation by Fe-impregnated biochar. *Chem. Eng. J.* **2020**, *385*, No. 123921.
(59) Lai, L.-D.; He, Y.-L.; Zhou, H.-Y.; Huang, B.-K.; Yao, G.; Lai, B. Critical review of natural iron-based minerals used as heterogeneous catalysts in peroxide activation processes: Characteristics, applications and mechanisms. *J. Hazard. Mater.* **2021**, *416*, No. 125809.
(60) Chen, Y.-F.; Miller, C. J.; Waite, T. D. Heterogeneous Fenton chemistry revisited: Mechanistic insights from ferrihydrite-mediated oxidation of formate and oxalate. *Environ. Sci. Technol.* **2021**, *55*, 14414−14425.
(61) Qin, Y.-X.; Zhang, L.-Z.; An, T.-C. Hydrothermal carbon-mediated Fenton-like reaction mechanism in the degradation of alachlor: Direct electron transfer from hydrothermal carbon to Fe(III). *ACS Appl. Mater. Interface* **2017**, *9*, 17115−17124.
(62) Feng, D.-Q.; Shou, J.-X.; Guo, S.; Ya, M.-N.; Li, J.-F.; Dong, H.-P.; Li, Y.-M. Co-catalysis of trace dissolved Fe(III) with biochar in hydrogen peroxide activation for enhanced oxidation of pollutants. *RSC Adv.* **2022**, *12*, 17237−17248.
(63) Liu, W.; Wang, Y.; Ai, Z.; Zhang, L. Hydrothermal synthesis of FeS_2 as a high-efficiency Fenton reagent to degrade alachlor via superoxide-mediated Fe(II)/Fe(III) cycle. *ACS Appl. Mater. Interface* **2015**, *7*, 28534−28544.
(64) Hassani, A.; Karaca, M.; Karaca, S.; Khataee, A.; Acisli, O.; Yilmaz, B. Preparation of magnetite nanoparticles by high-energy planetary ball mill and its application for ciprofloxacin degradation through heterogeneous Fenton process. *J. Environ. Manage.* **2018**, *211*, 53−62.

https://doi.org/10.1021/acsomega.3c07525
ACS Omega 2024, 9, 6595−6605